An Octet-Truss Engineered Concrete (OTEC) for Lightweight Structures

Parham Aghdasi[a*], Ian D. Williams[a], Brian Salazar[b], Nicole Panditi[b], Hayden K. Taylor[b], Claudia P. Ostertag[a]

[a] Department of Civil and Environmental Engineering, University of California, Berkeley, Berkeley, CA, USA

[b] Department of Mechanical Engineering, University of California, Berkeley, Berkeley, CA, USA

Abstract

Recent advances in the development of Ultra-High Performance Fiber-Reinforced Concrete (UHP-FRC) with very high compressive strength has inspired the development of a lightweight structure by engineering the void spaces in the material, thus taking advantage of porous concrete's thermal insulating properties while maintaining strength and stiffness. This paper refers to this engineered material as Octet-Truss Engineered Concrete (OTEC). To make OTEC structures, UHP-FRC and "green" UHP-FRC (G-UHP-FRC) mixtures were developed. 50.8-mm side-length OTEC unit cell specimens with various element diameters as well as 5×1×1-cell OTEC flexural specimens with 8 mm-diameter elements were cast and tested under uniaxial compression and four-point bending, respectively. The compressive strength of the OTEC unit cell specimens with various element diameters is mainly stretching-dominated, and hence considerably surpasses that of the control foam Green Ultra-High Performance Concrete specimens with random pore orientations. These results indicate a promising application of UHP-FRC and G-UHP-FRC OTECs for lightweight structures.

[*] Corresponding author. Email address: aghdasi@berkeley.edu (P. Aghdasi).

1. Introduction

Materials for energy-efficient building systems, such as façade and flooring systems, must have a balance of strength, stiffness, low weight, and thermal resistance. Finding the optimum balance of these properties leads to both structural and non-structural improvements throughout the building. Building energy consumption comprises almost half of all energy usage in the U.S., and 45% of this is used for heating, cooling, and ventilation [1]. The magnitudes of these numbers highlight the need for thermally resistant façade systems. Materials with high thermal resistance and sufficient strength enable adequate insulation while keeping the weight and thickness of the building envelope to a minimum. Façade and flooring systems make up a large portion of the dead load in a building; thus reductions in weight are reflected in the required structural system, particularly in earthquake-prone regions.

Foam concretes have been used for many years for lightweight, thermally resistant façades due to their low weight and good thermal properties. The most common method of producing foam concrete is the addition of aluminum powder, which reacts with calcium hydroxide in the cement paste to produce hydrogen bubbles resulting in a random pore structure throughout the cement matrix [2–4]. This random pore structure leads to an exponential decrease in strength and stiffness with increasing porosity, which is the main drawback of the use of foam concretes [5,6].

It is well known that cellular solids can deform in two ways: 1) bending or 2) stretching of the cell walls [7]. Poor mechanical performance of foam concretes is attributed to the stress flow in randomly distributed spherical pores. This type of microstructure is classified as bending-dominated. As shown in Figure 1, stresses applied to the material cause flexure in the pore walls that leads to the development of tensile stresses, causing a drop in the overall strength of the

foam since cement paste has poor tensile capacity compared to its compressive strength. Stretching-dominated lattices overcome this behavior by arranging the material such that all elements are subjected to predominantly axial stresses, as shown in Figure 1 [5]. Although most cellular solids are bending-dominated, those that are stretching-dominated are more efficient from a weight viewpoint for structural applications. This is because stretching-dominated cellular solids have a greater macroscopic modulus and initial yield strength compared to bending-dominated cellular materials of the same relative density. Stretching-dominated materials, however, have a softening post-yield response because of plastic buckling or brittle collapse of their struts [5], [8]. Stretching-dominated lattices, such as octet-truss lattices, have been proven to be effective for metals and ceramics [9–11]. Octet lattices seem to be ideal for concrete as well, especially if the concrete exhibits ultra-high compressive strength, since a compressive stress field places all elements in the lattice under compression. By arranging the material in this optimum pattern, higher strength and stiffness are achievable in an octet-truss lattice compared to foams with equivalent density.

In the last two decades, researchers have developed cementitious composites with ultra-high compressive strength (150 to 210 MPa) and ductility, more recently known as Ultra-High Performance Fiber-Reinforced Concrete (UHP-FRC). The current state-of-the-art [12,13] does not use any special materials or treatments to achieve ultra-high strength. In this research, ultra-high compressive strength was achieved via similar techniques to those used in prior research to develop UHP-FRC [12]. A simplified manufacturing process was employed, with no special treatments or materials while preserving high-packing density theory to optimize the types and proportions of the constituent materials. Interested readers are referred to [12,14] for more details. The selected constituent materials are all commercially available in the United States. In

addition, a new mix was designed in which 50% of Portland cement by weight was replaced with two industrial by-products, 25% fly ash (FA) class F and 25% ground granulated blast-furnace slag (GGBFS), to develop what is referred to as green UHP-FRC (G-UHP-FRC) to reduce its environmental impact. This article investigates the performance of both G-UHP-FRC and UHP-FRC OTECs, which could potentially be used in lightweight structures, such as energy-efficient building façade and flooring systems.

2. Materials and methods

2.1 Ultra-High Performance Fiber-Reinforced Concrete (UHP-FRC) and Green UHP-FRC (G-UHP-FRC)

Information for the materials used in the experimental program as well as mixture compositions are all summarized in Table 1. Flowability of the mixtures was examined according to ASTM C1437-07 [15], and compressive strengths of both 50.8-mm solid cube and OTEC unit cell material specimens were obtained in accordance with ASTM C109/109M-16 [16]. In both G-UHP-FRC and UHP-FRC mixtures, 0.5–2.0% by volume of 3 mm-long high modulus, ultra-high molecular weight polyethylene fibers of 38.4 μm diameter, with a tensile strength and elastic modulus of 2.2–2.4 GPa and 73–79 GPa, respectively, were introduced in order to obtain sufficient post-cracking toughness. Such short polyethylene fibers are desirable to ensure that the mixture is able to flow through the corners of the octet lattice mold without clogging during infiltration.

Compressive strengths of 110–140 MPa were achieved for G-UHP-FRC and UHP-FRC (Table 1) based on 50.8-mm solid cube specimens along with high flowability of more than 220 mm, which later proved to be essential for the extrusion of G-UHP-FRC and UHP-FRC into 3D-

printed octet lattice molds. The purpose of using UHP-FRC developed in prior research [12] was to enhance the compressive strength of OTEC unit cells, thereby providing a wider range of possibilities for future applications based on project requirements. UHP-FRC (Table 1), while using 100% cement, required a slightly higher water-to-cementitious materials ratio, W/CM ratio of 0.26, compared to prior research [12] in order to achieve sufficient flowability for proper infiltration of the 3D-printed octet lattice molds.

2.2 Octet lattice negative molds 3D-printed in Acrylonitrile Butadiene Styrene (ABS)

Creating the complex geometry of the octet-truss, illustrated in Figure 2a, from G-UHP-FRC or UHP-FRC, is difficult using traditional mold-making techniques. In recent years, however, additive manufacturing has enabled researchers and scientists to create complex geometries with great ease. In this study, negative octet molds, shown in Figure 2b, were 3D-printed in acrylonitrile butadiene styrene (ABS) using fused deposition modeling on a Stratasys Dimension 1200es printer. ABS filaments were deposited with a layer thickness of 0.1 mm to give a mold surface roughness that was tens of times smoother than the sizes of individual octet struts.

Each octet mold cavity contains multiple overhanging regions, so to prevent mold collapse during the layer-by-layer printing process, a pattern of soluble support material, Stratasys P400, was deposited into the cavities from the 3D printer's second extrusion nozzle. Once mold printing was complete, the support material was dissolved by placing the mold into a caustic lye bath (NaOH, with a concentration of about 2.0%) at 70°C for 2–3 days and then rinsing in tap water. This process resulted in a hollow mold prior to concrete infiltration.

Excellent flowability of G-UHP-FRC and UHP-FRC provided for the possibility of infiltrating these molds on a vibrating table, using a syringe as illustrated in Figure 2c. The printed mold

incorporated eight small funnels to serve as injection and air exhaust sites. Vibration as well as positive pressure applied by using a syringe during extrusion were the mechanisms used to remove entrapped air. The molds were designed with a wall thickness of 1 mm, making them dissolvable upon immersion in acetone after infiltration and solidification.

Figure 2d shows the final G-UHP-FRC/UHP-FRC OTEC unit cell after dissolving the ABS mold in acetone.

2.3 Dissolving the ABS molds in acetone

Upon adequate infiltration, the specimens were left to set in a fog room (with more than 95% relative humidity at room temperature) for about 24 hours, after which they were placed in an acetone bath at room temperature for 24–48 hours to dissolve away the ABS mold. Prior to using this manufacturing technique, the effect of acetone on the compressive strength of G-UHP-FRC was tested by placing three 50.8-mm solid cubes of G-UHP-FRC in an acetone bath for 24 hours and then testing them under compression. The compressive strengths of these cubes were compared to three control 50.8-mm solid cubes from the same batch that had not been placed in acetone. The average compressive strength of the samples exposed to acetone differed by less than about 3% from that of the control specimens, with the acetone-exposed specimens exhibiting the slightly higher average strength. These results sufficed to show that acetone does not adversely influence the mechanical properties of G-UHP-FRC and UHP-FRC.

2.4 Curing OTEC material specimens

After dissolving away the ABS molds, all material specimens, with the exception of a few, were placed in a fog room (with more than 95% relative humidity at room temperature) until a day before testing (usually at 28 days after casting). Although not quantified in this research, it is

believed that due to high particle packing density of the developed G-UHP-FRC/UHP-FRC, water permeation is limited to only a few millimeters from any exposed surface. Therefore, though water/moisture curing may not have a noticeable effect on the compressive strength development of 50.8-mm solid cube specimens, it was believed that it would most likely affect strength development of OTEC unit cell elements since the diameter sizes varied from only 8 to 12 mm, allowing water and moisture to penetrate the elements almost all the way through.

Hence, in order to investigate the effects of different types of water/moisture curing on the compressive strength development of the OTEC unit cells, eight specimens with 8 mm-diameter elements were made and cured using three different methods for comparison purposes. Two specimens were cured at room temperature and humidity as control samples, three specimens were cured in the fog room, and three more were immersed in water, all of which were removed from their curing environment a day before testing (at 28 days after casting).

2.5 Uniaxial compression tests of OTEC material specimens

Throughout this research, $(50.8\ \text{mm})^3$ OTEC unit cell material specimens were made with four different element diameters of 8, 10, 11, and 12 mm, resulting in void fractions (porosities) of 66.4, 53.6, 47.5, and 41.9%, respectively, as compared to a 50.8-mm solid cube. These OTEC unit cells were tested under compression using holders whose geometries were customized for each element diameter. In most cases the holders were milled from 6061 aluminum, as shown in Figure 3. The purpose of using a holder is to properly restrain the nodes of the truss from lateral displacement, and thus simulate the stress state that exists in octet lattice structures having many cells in at least two directions, as would be found, for example, in an OTEC panel. Large two- or three-dimensional arrays of OTEC cells are almost completely stretching-dominated structures,

and when loaded compressively at their largest two opposing boundaries (*e.g.* on opposite sides of a panel), all their struts experience largely uniaxial compressive loads. In contrast, if a single isolated experimental octet unit cell, or just a few cells, were to be loaded without lateral constraints, relatively large flexural as well as tensile loads would be induced in some elements, leading to behavior that would not be representative of that anticipated in larger built structures.

In addition to OTEC unit cell material specimens, companion G-UHP-FRC and UHP-FRC 50.8-mm solid cube material specimens were made and tested under compression for comparison purposes, the results of which are all presented in Section 3.1.

Four sets of OTEC unit cell material specimens were made and tested under compression throughout this research. In the first set of experiments, nine OTEC unit cells with 8, 10, and 12 mm-diameter elements were made using G-UHP-FRC (Table 1) in order to quantify the effects of varying the void fraction of an OTEC unit cell on its compressive strength. These samples were later tested under uniaxial compression using 3D-printed ABS holders. Soon, it was realized that these ABS holders were not very effective in restraining the nodes since multiple cracks were induced in the holders during testing. Therefore, for the remaining set of experiments, the holders were machined from 6061 aluminum, as mentioned above.

In the first set of experiments, two 50.8-mm foam G-UHPC cubes with a void fraction of 45.3% were also made and tested under compression, for comparison purposes with OTEC unit cells. Foaming was induced by aluminum powder that was added to G-UHPC during the mixing procedure. Aluminum powder reacts with the hydration products, especially calcium hydroxide, and results in the formation of tricalcium aluminate hydrate and hydrogen gas, which introduces entrapped air bubbles throughout the matrix.

In the second set of experiments, UHP-FRC (Table 1), using 100% cement and a slightly higher W/CM ratio of 0.26, was used to make six OTEC unit cell material specimens with 8 mm-diameter elements. The purpose of this experiment was to investigate the effects of three different fiber volume fractions (0.5, 1.0, and 1.5%) on the flowability of their matrices as well as the compressive strengths and post-cracking behavior of the OTEC unit cells. It should be noted here that in a few instances in this experiment, some flexural cracks were observed in a few elements that were attributed to the lack of sufficient depth of the top piece of the aluminum holder, thus allowing for some of the top nodes to slide transversely, inducing flexural moments. Therefore, for the rest of the experiments, the holder design was revised to include a deeper top piece, ensuring that all top nodes were properly restrained from any transverse displacement.

In the third set of experiments, UHP-FRC (Table 1) was used to make eight more OTEC unit cells with 8 mm-diameter elements to explore the effects of water/moisture curing on their compressive strength development as also mentioned in Section 2.4.

In the fourth set of experiments, it was decided to continue using UHP-FRC with 0.5% volume fraction of fibers to make and test twelve more OTEC unit cells with 8, 10, and 11 mm-diameter elements in order to duplicate the results thus far achieved, by once more quantifying the effects of varying the void fraction of an OTEC unit cell on its compressive strength.

The G-UHP-FRC 50.8-mm solid cube, foam cube, as well as 8,10, and 11 mm OTEC unit cell material specimens are all illustrated in Figure 4. In addition, using UHP-FRC, a 3×3×1-cell OTEC panel with 8 mm-thick flanges on both sides and 8 mm-diameter elements, which is shown in Figure 5a, was cast successfully without any visible surface voids or defects.

Furthermore, it was desired to understand whether the dependence of compressive strength on void fraction that was observed in Experiments #1 and #4 could also be seen with a polymeric material and in structures with a higher confidence of having no surface or internal void defects. Therefore, three further octet lattice unit cells with 8, 10, and 11 mm-diameter elements as well as a 50.8-mm solid cube were directly printed from the polymer polylactic acid (PLA) using a Type A Pro fused deposition modeling machine. These samples were also then tested under uniaxial compression (Experiment #5).

For the first two sets of experiments, the OTEC unit cells were tested under compression using a hydraulic load-controlled machine with a constant loading rate of 1.5 kN/sec, while, for the last three experiments, all specimens were tested using a displacement-controlled machine at a constant displacement rate of 6 mm/min. The latter approach allowed for recording the cross-head displacement, from which compressive load–strain curves were generated.

In addition, theoretical strength values for 8, 10, and 11 mm UHP-FRC OTEC unit cells were calculated using the structural analysis software package OpenSees [17], where two formulations were used to model the specimens for comparison purposes. The first, and simplest, model uses pinned truss elements and a brittle material model. In this model, each member of the OTEC specimen is modeled with a single truss element. This type of model is most commonly used to predict the strength of structures with slender elements, as flexural behavior has only a minor effect on such elements and is often neglected. The second formulation uses a force-based beam-column element with a circular fiber section at each integration point and a brittle material model. Each member is divided into four beam-column elements to improve accuracy. This model is better suited to less slender elements because it accounts for flexural behavior in the elements, though it neglects shear deformations. Horizontal displacements and all rotations were

restrained in the nodes for all three specimens to mimic the boundary conditions imposed by the aluminum holders used in the experimental tests. Vertical displacement was restrained in the bottom nodes and imposed on the top nodes by the displacement-controlled integrator used in analysis.

2.6 Four-point bending tests of G-UHP-FRC 5×1×1-cell OTEC and solid control flexural material specimens

In addition to OTEC unit cells tested under uniaxial compression, four G-UHP-FRC 5×1×1-cell OTEC flexural material specimens with 8 mm-thick flanges on both sides and 8 mm-diameter elements were cast using 3D-printed ABS molds. One of these specimens is illustrated in Figure 5b. The specimens were then tested under four-point bending in order to characterize their flexural behavior. Figure 6 illustrates the test setup and its dimensions. One of the four G-UHP-FRC specimens was cured at room temperature and humidity while the rest of the specimens were cured in the fog room (with more than 95% relative humidity at room temperature) until a day before testing. For comparison purposes, two solid UHP-FRC (Table 1) control specimens were also made, one with the same dimensions (50.8 mm×50.8 mm×222.0 mm) and one with the same mass (26.7 mm×50.8 mm×222.0 mm) as those of the G-UHP-FRC 5×1×1-cell OTEC flexural material specimens. To add to this comparison, another solid control specimen (50.8 mm×50.8 mm×222.0 mm) was cast using conventional concrete (Table 1). All control specimens were also cured in the fog room until a day before testing.

3. Results and discussion

An overview of the experimental program of this research is illustrated in the flowchart given in Figure 7.

3.1 Uniaxial compression tests of OTEC material specimens

Compression test results of all of the OTEC unit cells as well as 50.8-mm foam and solid G-UHP-FRC and UHP-FRC cubes after 28 days of curing (unless otherwise specified) are summarized in Table 2.

The results of the first set of experiments show that it is possible to obtain much higher compressive strengths from G-UHP-FRC OTEC unit cells than from foam G-UHPC cubes with a comparable void fraction. As later confirmed in the fourth and fifth set of experiments, it was further noticed that an OTEC unit cell with 8 mm-diameter elements (referred to as the "8 mm OTEC" in Table 2) demonstrates a higher specific compressive strength than that of an estimation expected from a log–log regression based on the strength values of the other specimens with lower porosities (*i.e.* the 10 and 12 mm OTEC unit cells and the 50.8-mm solid cube). Therefore, for the next two experiments (Experiments #2 and #3), 8 mm OTEC unit cells were used to further study the effects of various fiber volume fractions and different curing methods on their compressive strengths. In addition, these experiments were carried out with the aim of further enhancing the compressive strengths of the 8 mm OTEC unit cells beyond 10 MPa.

In the second set of experiments, the effects of fiber volume fraction on both fresh and hardened properties were investigated, and as the results in Table 2 suggest, a somewhat linear reduction in strength, as well as flowability (not measured quantitatively, but observed qualitatively) is noticed with an increase in the fiber volume fraction for both the solid cubes and 8 mm OTEC unit cells. This effect is believed to be due to the fact that reduced flowability is more likely to

result in more entrapped air and small defects, thus lowering the strength. The fibers do, however, increase post-cracking toughness by adding more ductility to the matrix.

In the third set of experiments, in which three different methods of curing were employed, a 40% increase in compressive strength was achieved by curing the 8 mm UHP-FRC OTEC unit cells in the fog room versus under regular room conditions. This pronounced effect gives validity to the earlier assumption made in Section 2.4 that, since the strut diameter is only 8 mm, water and moisture are able to penetrate sufficiently far into the elements to allow for a higher degree of cement hydration. The goal of reaching more than 10 MPa in compressive strength was accomplished for all of the specimens that were either cured in the fog room or immersed in water, which are indicated in bold in Table 2. Although all material specimens were removed from their curing environment and moved to room temperature and humidity a day before testing, this does not appear to have led to the elements drying out internally. After compressive testing, fragments of all OTEC unit cells that had been either immersed in water or kept in the fog room, were examined visually, and the UHP-FRC was seen to be still wet inside, further confirming the penetration of water into the elements. A slightly lower average compressive strength (~4% lower) was measured for the OTEC unit cells that had been immersed in water compared to those cured in the fog room, but this difference is not statistically significant as indicated by a one-sided Student's t-test performed at the 5% level of significance.

The load–strain curves for all 8 mm UHP-FRC OTEC unit cells tested during this experiment are shown in Figure 8. Figure 8d further demonstrates higher stiffness, peak load, strain at peak (higher ductility), and toughness for the material specimens that were either cured in the fog room or immersed in water compared to those that were merely kept at room temperature and humidity.

According to the results of the fourth set of experiments, compressive strengths well beyond 10 MPa were measured for all four 8 mm OTEC unit cells. An average increase of 38% and 77% in compressive strength were obtained for 10 and 11 mm OTEC unit cells, respectively, compared to 8 mm OTEC unit cells. As for the failure mode of the UHP-FRC OTEC unit cells tested in Experiments #3 and #4, all diagonal elements experienced columnar failure under compression characterized by development of tensile cracks along the direction of these elements. UHP-FRC, like other types of concrete, is much weaker in tension than in compression (~1/10); thus, when a UHP-FRC element is tested under compression, its lateral expansion (due to Poisson's effect) followed by development of lateral tensile stresses ultimately results in the formation of tensile cracks along the direction of the applied compressive force. This phenomenon explains the formation of cracks along the diagonal elements of the UHP-FRC OTEC unit cells (Figure 9a) as well as the vertical cracks that were observed after testing the 50.8-mm solid UHP-FRC cube specimens (Figure 9b) under uniaxial compression. The stress-strain response of UHP-FRC, with 0.5% volume fraction of PE fibers, under uniaxial compression is shown in Figure 10, and Figure 11 illustrates all of the load–strain curves of the UHP-FRC OTEC unit cells tested in this experiment, the averages of which are all included in Figure 11d along with the foam G-UHPC cube tested in the first experiment.

Although all of the three 8, 10, and 11 mm UHP-FRC OTEC unit cells have a higher porosity (66.4, 53.6, and 47.5%, respectively) compared to the foam G-UHPC cube (45.3% porosity), they all obtained much higher peak loads, strains at peak, and toughness, verifying the efficiency of the UHP-FRC OTEC unit cells in regard to their performance under uniaxial compression.

In the fifth set of experiments, average increases of 63% and 133% in compressive strength were obtained for 10 and 11 mm PLA lattice cells, respectively, compared to the 8 mm PLA lattice

cell. The failure of the PLA octet lattice cells was largely dominated by the flexural moments that were induced at the ends of each of the diagonal elements, resulting in double-curvature of these elements. It should be noted that the PLA solid cube did not fail at the end, and the test had to be stopped to avoid any damage to instrumentation. For comparison purposes, however, its load at 45% compressive strain (close to that reached by the 10 and 11 mm PLA lattice cells) was used to calculate its compressive strength.

A summary of the results of the first, fourth, and the fifth experiments is plotted, similar to that of [18], in Figure 12, which shows compressive strength versus density with log–log scaling. As also expressed earlier, what is apparent is that the 8 mm octet lattice cell, for all these three experiments, performs better than would be estimated from a log–log regression based on the strength values of the other specimens with lower porosities (*i.e.* the 10 and 11 mm lattice cells and the 50.8-mm solid cube). A similar claim could also be made for the 10 mm octet lattice compared to the 11 mm (or 12 mm) lattice cell and the solid cube. This effect is attributed to two factors: 1) the smaller the strut or element diameter, the less material is used per unit of lattice cell volume, resulting in a lower probability of containing defects above a certain size which would weaken the lattice elements, and 2) an octet lattice cell with more slender elements (8 mm compared to 10 and 11 mm lattice cells) is presumably more stretching-dominated, and hence, experiences much less shear and flexural moments at the nodes. Further investigation of this matter will be the subject of future research.

Table 3 summarizes the estimated compressive strengths for all of the specimens based on a log–log regression using the last three data points (the 10 mm, 11 mm [or 12 mm] lattice cells, and solid cubes). As the errors in Table 3 show, this regression considerably underestimates the compressive strengths of the 8 mm octet lattice cells. It is also worth noting that these errors are

much smaller for the PLA lattice cells and solid cube (Experiment #5): this difference is expected, since 3D-printing PLA will have presumably resulted in lower defect densities in the components produced than the casting of the G-UHP-FRC and UHP-FRC OTEC unit cell specimens.

The suggestion that higher void fractions give higher specific strengths is further explored in Figure 13, where relative density is plotted against normalized compressive strength. Here, the performances of different octet lattice cells as well as the foam G-UHPC and solid cube specimens, tested in Experiments #1, #4, and #5, are compared with the limit of stretching-dominated as well as bending-dominated ideal behaviors.

The stretching-dominated ideal limit, with a logarithmic slope of 1.0 [5], interpolates between the extreme cases of 100% of the potential compressive strength obtained at 0% porosity (this is the case for 50.8-mm solid G-UHPC, G-UHP-FRC, UHP-FRC, and PLA cubes) and zero strength at 100% porosity (as with air). The bending-dominated ideal behavior has a theoretical logarithmic slope of 1.5 [5]. It is apparent that all OTEC unit cells diverge less from the ideal behavior than foam G-UHPC cubes, and among the octet lattice cells, the 8 mm design, as expected, deviates the least from ideal behavior. In addition, by comparing the plots for the PLA octet lattice unit cells with those of UHP-FRC OTEC unit cells, a very similar normalized performance trend is noticed for the two types of materials, which is not only an indication of the validity of the tests and reproducibility of the results for different materials, but more importantly is an indication of an expected normalized performance for the UHP-FRC OTEC unit cells similar to that of a polymeric material with a higher certainty of having no surface or internal void defects.

According to Figure 13, it is observed that the first OpenSees [17] model with pinned truss elements, thus only allowing for axial forces in the elements, results in a linear behavior just below the bending-dominated ideal behavior. Therefore, even with a defect-free model under pure axial compressive forces, for brittle materials, it is not possible to reach any of the ideal behaviors. Using beam-column elements in the second OpenSees [17] model allowed for the development of bending moments in the elements. This leads to a behavior that results from both stretching and bending. The stretching effect, however, is more pronounced as the elements become more slender. This is observed for both the second model as well as the experiments (Experiments #5 and #6) for the 8 mm octet lattice cell since its behavior deviates from the trend of other designs with less slender elements and towards the behavior of the first model with pinned truss elements. In general, very comparable trend and normalized compressive strength values were calculated for the 8, 10, and 11 mm UHP-FRC OTEC unit cells using beam-column elements, by considering the effects of bending moments, in OpenSees [17], which again gives validity to the experimental tests.

3.2 Four-point bending tests of G-UHP-FRC 5×1×1-cell OTEC and solid control flexural material specimens

The load–deflection curves of the three G-UHP-FRC 5×1×1-cell OTEC flexural material specimens under four-point bending are illustrated in Figure 14. For all these three specimens, the failure mode was primarily dominated by flexure (compared to shear as another possible failure mode often observed for flexural specimens with small span-to-depth ratios). Higher peak loads (an average increase of 97%), initial stiffness, and toughness were recorded for the two specimens that were cured in the fog room (with more than 95% relative humidity at room temperature) compared to the one cured at room temperature and humidity. This effect is

compatible with the results of the 8 mm UHP-FRC OTEC unit cells, cured using three different methods and tested under uniaxial compression in the third set of experiments (Figure 8), presented in Section 3.1.

In Figure 15, the load–deflection curves of G-UHP-FRC 5×1×1-cell OTEC flexural material specimens are plotted on the same graph as the load–deflection curves for the control specimens, including the solid conventional concrete flexural specimen (Table 1) with the same external volume; the solid UHP-FRC flexural specimen with the same external volume; and the solid UHP-FRC flexural specimen with the same mass. The fourth G-UHP-FRC 5×1×1-cell OTEC flexural material specimen performed slightly better than the average of the two specimens that were cured in the fog room, due to some minor changes in the mix design and also its older age. The peak load, midpoint deflection at peak, as well as toughness (area under the load–deflection curves) values are also summarized in Table 4. It is observed that the G-UHP-FRC OTEC flexural specimens were able to achieve up to 65 and 71% of the toughness of the solid UHP-FRC flexural specimen with the same volume, while only having a mass of about 53% of that of this solid specimen. An increase in toughness of about 254 and 283% were achieved for the G-UHP-FRC OTEC flexural specimens as compared to the solid UHP-FRC flexural specimen with the same mass. Similarly, the G-UHP-FRC OTEC flexural specimens obtained an increase in toughness of about 85 and 100% as compared to the solid conventional concrete flexural specimen (Table 1) with the same volume, while also reaching 73 and 94% of its peak load under flexure. These results suffice to illustrate the excellent performance of the G-UHP-FRC OTEC specimens under flexure.

4. Summary and conclusions

By using a simple manufacturing process and implementing the high-packing density theory, ultra-high compressive strengths of up to more than 120 MPa and 140 MPa were obtained after 28 days based on 50.8-mm solid cube material specimens for mixtures using 50% and 100% Portland cement, respectively (refer to Table 1). In the former mixture, referred to as G-UHP-FRC, 50% of cement by weight was replaced with two industrial by-products, 25% FA and 25% GGBFS. The latter mixture, namely UHP-FRC, using 100% Portland cement, was later developed to further improve the compressive strength of the material. By implementing a few minor changes in the mix design and using a W/CM ratio of 0.26, slightly higher than that of prior research [12], a flow diameter of 224 mm was obtained. This modified mixture proved sufficient for extrusion into 3D-printed octet lattice molds. Using both of these mixtures, G-UHP-FRC and UHP-FRC, much higher compressive strengths were recorded for OTEC unit cells compared to foam G-UHPC cubes. For example, the compressive strength values of the OTEC unit cell specimens with various element diameters (8, 10, and 11 mm resulting in 66.4, 53.6, and 47.5% porosity, respectively) tested in Experiment #4 considerably exceeded that of the control foam G-UHPC specimens (45.3% porosity) with a geometrically disordered pore structure (by about 180, 290, and 400%, respectively). All of the constituent materials used in this research are commercially available in the U.S. market. To summarize, the following conclusions can be drawn from this research:

1. Increasing the volume fraction of PE fibers (Table 1) from 0.0 to 2.0% leads to a fairly linear reduction in flowability of UHP-FRC and compressive strength of both UHP-FRC solid cubes and OTEC unit cells.
2. For UHP-FRC OTEC specimens with 8 mm-diameter elements, up to about a 40% increase in compressive strength and a 97% increase in flexural capacity as well as higher

stiffness and toughness could be achieved by curing OTEC specimens in a fog room with more than 95% relative humidity at room temperature. This effect is believed to be due to a higher degree of cement hydration as a result of sufficient water permeability into the first few millimeters from any exposed surface of the UHP-FRC.

3. Average compressive strength above 12 MPa was recorded for 8 mm UHP-FRC OTEC unit cells, compared to which an average increase of 38% and 77% was obtained for 10 and 11 mm UHP-FRC OTEC unit cells, respectively. These different lattice geometries therefore offer a wide range of strengths for different applications and requirements. Furthermore, the greater efficiency of the UHP-FRC OTEC unit cells (with 8, 10, and 11 mm-diameter elements resulting in 66.4, 53.6, and 47.5% porosity, respectively), in regard to peak load, strain at peak, and toughness under uniaxial compression was verified compared to that of foam G-UHPC cubes (45.3% porosity).
4. Octet lattice cells with higher porosity, and thus lower density reach compressive strength values that are much closer to the ideal than those attained by specimens with lower porosities. This difference is attributed to two factors: 1) an 8 mm lattice cell uses less material per unit of lattice cell volume compared to 10 and 11 mm lattice cells, leading to a lower probability of containing defects larger than a given size and hence low-strength components, and 2) an octet lattice cell that uses more slender elements (8 mm compared to 10 and 11 mm lattice cells) undergoes much less shear and flexural moments at the nodes due to a more stretching-dominated mechanism.
5. A similar normalized performance trend was observed for both PLA octet lattice unit cells and UHP-FRC OTEC unit cells, testifying to the reproducibility of the results for different materials as well as creating confidence in the normalized results recorded for

the UHP-FRC OTEC unit cells similar to that of a polymeric material with a higher certainty of having no surface or internal void defects.

6. By modeling the UHP-FRC OTEC unit cells in OpenSees [17], it was observed that even with a defect-free model for brittle materials under pure axial compressive forces, using pinned truss elements, it is impossible to reach any of the ideal behaviors. Using beam-column elements in the model, however, allows for the development of bending moments in the elements, which results in a behavior due to both stretching and bending. The stretching effect, however, is more prominent as the elements become more slender. This was observed for the 8 mm octet lattice cell (with the most slender elements) for both the second OpenSees [17] model, using beam-column elements, as well as the experiments (Experiments #5 and #6).
7. Up to 71 and 100% of the toughness of the solid UHP-FRC and conventional concrete flexural specimens, respectively, was achieved with the G-UHP-FRC OTEC flexural specimen with the same volume while also reaching 94% of the peak load of the solid conventional concrete specimen under flexure, only having a mass of about 53–55% of that of these solid specimen. Such UHP-FRC and G-UHP-FRC OTEC structures encased between skins would entrap air and potentially provide excellent thermal and acoustic insulation, the study of which will be the subject of future work.

Based on these results, utilizing G-UHP-FRC and UHP-FRC OTECs (such as 50.8-mm side-length OTEC cells with 8 mm-diameter elements [porosity of 66.4%] as studied extensively in this research), is recommended for lightweight façade and flooring systems. The application of OTECs could very well be extended to load-bearing structural systems, such as space trusses, concrete shells, shear walls, and the like, which will be investigated in the future.

Acknowledgements

The authors gratefully acknowledge the assistance of the staff of the Jacobs Institute for Design Innovation at U.C. Berkeley. The authors would also like to express their appreciation to Minifibers, Inc. for donating fibers. This research is funded by the Republic of Singapore's National Research Foundation through a grant to the Berkeley Education Alliance for Research in Singapore (BEARS) for the Singapore-Berkeley Building Efficiency and Sustainability in the Tropics (SinBerBEST) Program. BEARS has been established by the University of California, Berkeley, as a center for intellectual excellence in research and education in Singapore.

References

[1] Sung D. A New Look at Building Facades as Infrastructure. Engineering 2016;2:63–8.
[2] Melo JP, Aguilar AS, Olivares francisco H. Cement Paste Foamed by the Addition of Aluminum Powder with Metakaolin and Sepiolite. Constr. Build. Res., 2014, p. 443–51. doi:10.1007/978-94-007-7790-3_54.
[3] Ramamurthy K, Kunhanandan Nambiar EK, Indu Siva Ranjani G. A classification of studies on properties of foam concrete. Cem Concr Compos 2009;31:388–96. doi:10.1016/j.cemconcomp.2009.04.006.
[4] Tonyan TD, Gibson LJ. Strengthening of cement foams. J Mater Sci 1992;27:6379–86. doi:10.1007/BF00576288.
[5] Ashby MF. The properties of foams and lattices. Philos Trans A Math Phys Eng Sci 2006;364:15–30. doi:10.1098/rsta.2005.1678.
[6] Nambiar EKK, Ramamurthy K. Models for strength prediction of foam concrete. Mater Struct 2008;41:247–54. doi:10.1617/s11527-007-9234-0.
[7] Deshpande VS, Ashby MF, Fleck NA. Foam topology: bending versus stretching dominated architectures. Acta Mater 2001;49:1035–40. doi:10.1016/S1359-6454(00)00379-7.
[8] Deshpande VS, Fleck NA, Ashby MF. Effective properties of the octet-truss lattice material. J Mech Phys Solids 2001;49:1747–69. doi:10.1016/S0022-5096(01)00010-2.
[9] Bauer J, Hengsbach S, Tesari I, Schwaiger R, Kraft O. High-strength cellular ceramic composites with 3D microarchitecture. Proc Natl Acad Sci U S A 2014;111:2453–8. doi:10.1073/pnas.1315147111.
[10] Bückmann T, Stenger N, Kadic M, Kaschke J, Frölich A, Kennerknecht T, et al. Tailored 3D mechanical metamaterials made by dip-in direct-laser-writing optical lithography. Adv Mater 2012;24:2710–4. doi:10.1002/adma.201200584.
[11] Zheng X, Lee H, Weisgraber TH, Shusteff M, DeOtte J, Duoss EB, et al. Ultralight, Ultrastiff Mechanical Metamaterials. Science (80-) 2014;344:1373–7.

doi:10.1126/science.1252291.
[12] Aghdasi P, Heid AE, Chao SH. Developing ultra-high-performance fiber-reinforced concrete for large-scale structural applications. ACI Mater J 2016;113:559–69. doi:10.14359/51689103.
[13] Wille K, Naman AE, Parra-Montesinos GJ. Ultra - High Performance Concrete with Compressive Strength Exceeding 150 MPa (22ksi) : A Simpler Way. ACI Mater J 2011;108:46–53. doi:10.14359/51664215.
[14] Naaman A, Wille K. Some correlation between high packing density, ultra-high performance, flow ability, and fiber reinforcement of a concrete matrix. BAC2010—2nd Iber Congr Self Compact 2010.
[15] ASTM C1437-07, Standard Test Method for Flow of Hydraulic Cement Mortar. West Conshohocken, PA: ASTM International; 2007.
[16] ASTM C109/C109M-11a, Standard Test Method for Compressive Strength of Hydraulic Cement Mortars (Using 2-in. or [50-mm] Cube Specimens). West Conshohocken, PA: ASTM International; 2016.
[17] McKenna F, Fenves G, Scott M, Jeremic B. Open system for earthquake engineering simulation (OpenSees) 2000.
[18] Ashby M. Materials Selection in Mechanical Design. 3rd ed. Butterworth-Heinemann; 2005.

Figures

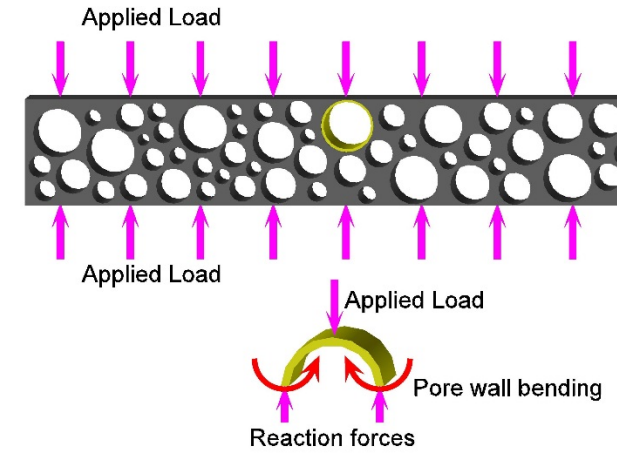

(a)

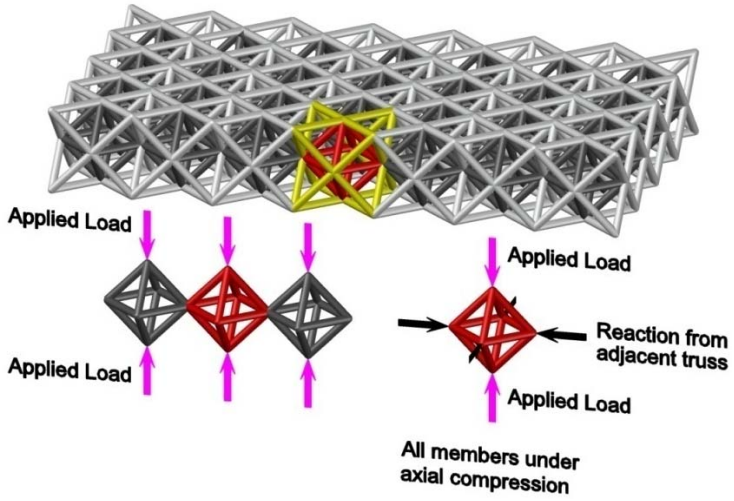

(b)

Figure 1 - (a) Bending of pore walls in foams (bending-dominated) and (b) stress flow in stretching-dominated lattices (octet-truss lattice).

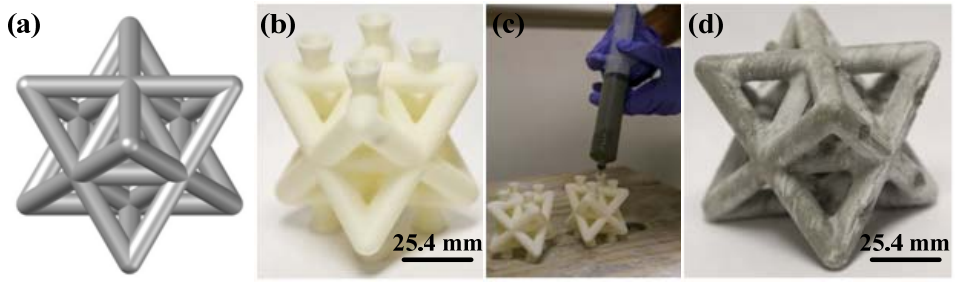

Figure 2 - (a) Schematic drawing of an octet lattice unit cell, (b) 3D-printed octet lattice unit cell ABS mold, (c) infiltrating molds on a vibrating table, and (d) final G-UHP-FRC/UHP-FRC OTEC unit cell.

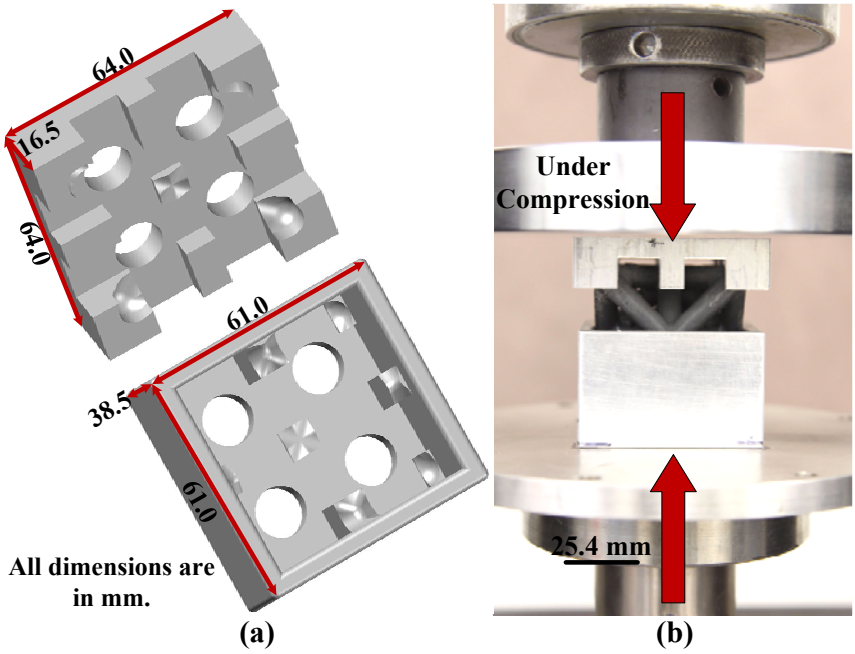

Figure 3 - (a) Aluminum holder for compression test of OTEC unit cell material specimens and (b) an OTEC unit cell with 8 mm-diameter elements under compression using the aluminum holders.

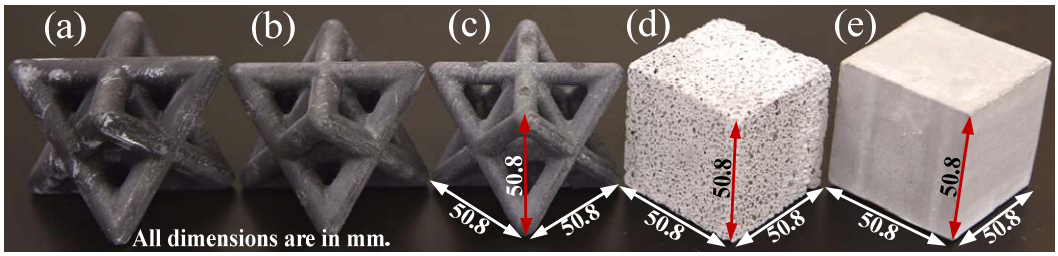

Figure 4 - 50.8-mm side-length UHP-FRC OTEC unit cell material specimens with (a) 11, (b) 10, and (c) 8 mm-diameter elements and (d) 50.8-mm foam G-UHPC cube and (e) 50.8-mm solid G-UHP-FRC cube material specimens before testing under uniaxial compression.

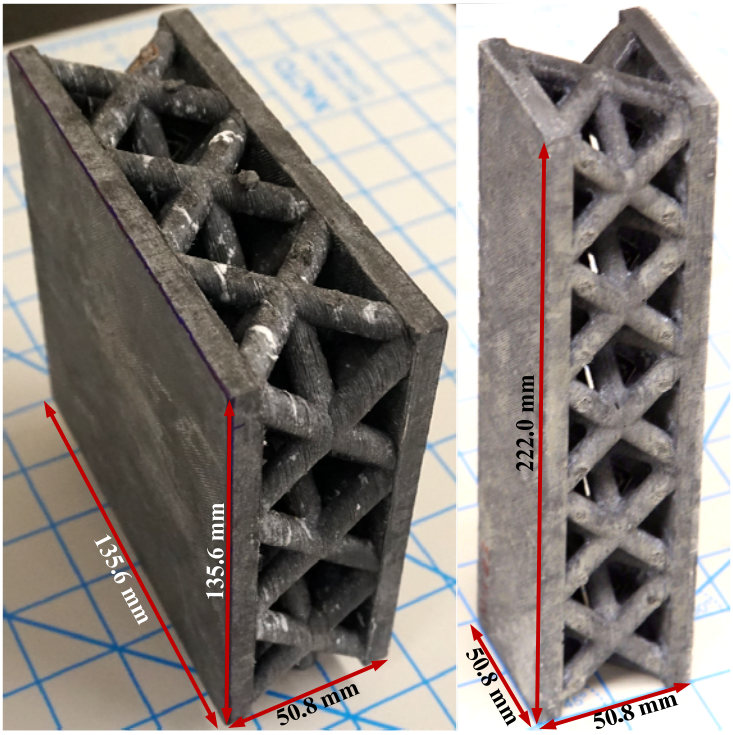

Figure 5 - (a) 3×3×1-cell OTEC panel showing surface defect-free production (mechanical testing results are not reported in this work) and (b) 5×1×1-cell OTEC flexural material specimen.

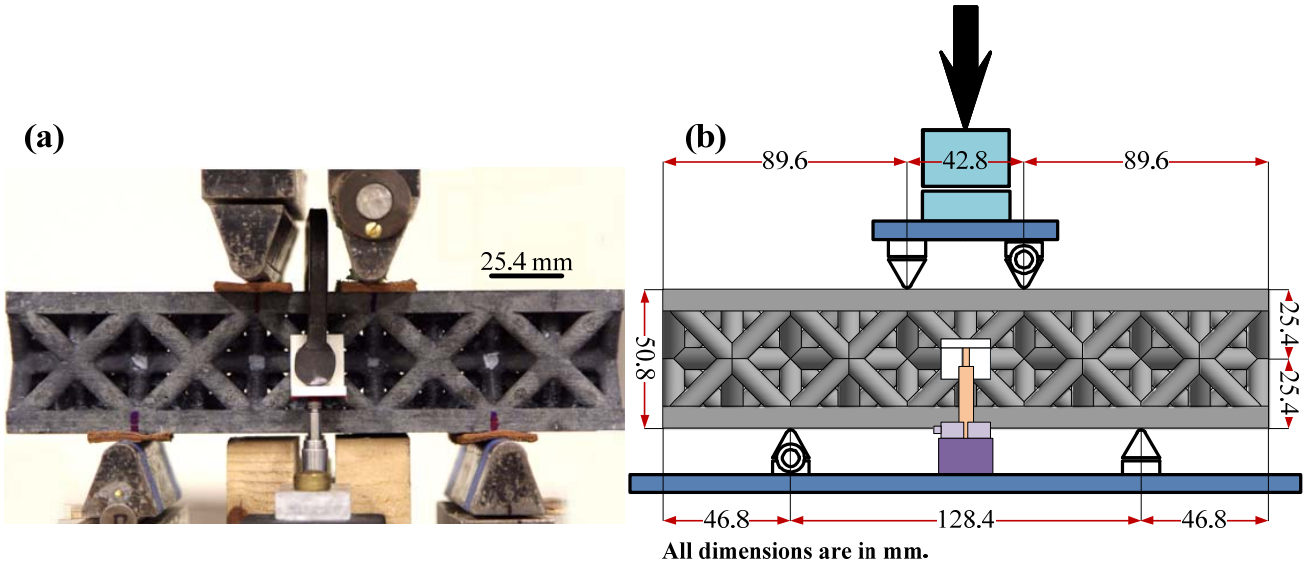

Figure 6 - (a) Actual and (b) schematic design of the four-point bending test setup (As illustrated in the photo, a C-clamp was used to attach a 3D-printed PLA angle to the middle node on both sides of the beam to allow for deflection measurements using a linear variable differential transformer [LVDT]).

Experimental Program

Compression Tests*

	Experiment #1	Experiment #2	Experiment #3	Experiment #4	Experiment #5
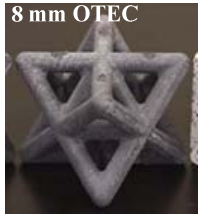	**8 mm OTEC** 3 unit cells ABS mold G-UHP-FRC 66.4% porosity 2.0% fibers Cured in fog room ABS holders Strength = 7.1 MPa	**8 mm OTEC** 2 unit cells ABS mold UHP-FRC 66.4% porosity 0.5% fibers Cured in fog room Aluminum holders #1 Strength = 5.7 MPa	**8 mm OTEC** 2 unit cells ABS mold UHP-FRC 66.4% porosity 0.5% fibers Cured in room Aluminum holders #2 Strength = 8.4 MPa	**8 mm OTEC** 4 unit cells ABS mold UHP-FRC 66.4% porosity 0.5% fibers Cured in fog room Aluminum holders #2 Strength = 12.1 MPa	**8 mm Octet Lattice** 1 unit cell 3D-Printed PLA 66.4% porosity Aluminum holders #2 Strength = 5.7 MPa
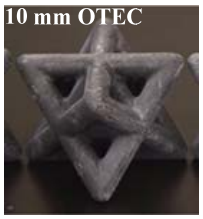	**10 mm OTEC** 3 unit cells ABS mold G-UHP-FRC 53.6% porosity 2.0% fibers Cured in fog room ABS holders Strength = 10.2 MPa	**8 mm OTEC** 2 unit cells ABS mold UHP-FRC 66.4% porosity 1.0% fibers Cured in fog room Aluminum holders #1 Strength = 5.5 MPa	**8 mm OTEC** 3 unit cells ABS mold UHP-FRC 66.4% porosity 0.5% fibers Cured in fog room Aluminum holders #2 Strength = 11.8 MPa	**10 mm OTEC** 4 unit cells ABS mold UHP-FRC 53.6% porosity 0.5% fibers Cured in fog room Aluminum holders #2 Strength = 16.7 MPa	**10 mm Octet Lattice** 1 unit cell 3D-Printed PLA 53.6% porosity Aluminum holders #2 Strength = 9.3 MPa
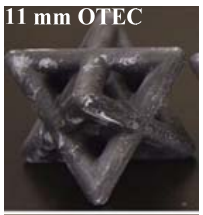	**12 mm OTEC** 3 unit cells ABS mold G-UHP-FRC 41.9% porosity 2.0% fibers Cured in fog room ABS holders Strength = 16.6 MPa	**8 mm OTEC** 2 unit cells ABS mold UHP-FRC 66.4% porosity 1.5% fibers Cured in fog room Aluminum holders #1 Strength = 4.8 MPa	**8 mm OTEC** 3 unit cells ABS mold UHP-FRC 66.4% porosity 0.5% fibers Cured in water Aluminum holders #2 Strength = 11.3 MPa	**11 mm OTEC** 4 unit cells ABS mold UHP-FRC 47.5% porosity 0.5% fibers Cured in fog room Aluminum holders #2 Strength = 21.4 MPa	**11 mm Octet Lattice** 1 unit cell 3D-Printed PLA 47.5% porosity Aluminum holders #2 Strength = 13.3 MPa
	**50.8-mm foam** 2 cubes G-UHPC 45.3% porosity 2.0% fibers Cured in fog room Strength = 16.6 MPa				

Flexural Tests

8 mm OTEC 1 5×1×1-cell 8 mm flanges 50.8×50.8×222.0 mm^3 ABS mold G-UHP-FRC 47% porosity 1.5% fibers Cured in room Max load = 1.9 kN Deflection at peak = 0.38 mm	**Solid #1** 1 prism 50.8×50.8×222.0 mm^3 Conventional concrete 0% porosity 0% fibers Cured in fog room Max load = 4.9 kN Deflection at peak = 0.38
8 mm OTEC 2 5×1×1-cell 8 mm flanges 50.8×50.8×222.0 mm^3 ABS mold G-UHP-FRC 47% porosity 1.5% fibers Cured in fog room Max load = 3.6 kN Deflection at peak = 0.31 mm	**Solid #2** 1 prism 50.8×50.8×222.0 mm^3 UHP-FRC 0% porosity 0% fibers Cured in fog room Max load = 8.5 kN Deflection at peak = 0.61
8 mm OTEC 1 5×1×1-cell 8 mm flanges 50.8×50.8×222.0 mm^3 ABS mold G-UHP-FRC 47% porosity 1.5% fibers Cured in fog room Max load = 4.6 kN Deflection at peak = 0.52 mm	**Solid #3** 1 prism 26.7×50.8×222.0 mm^3 UHP-FRC 0% porosity 0% fibers Cured in fog room Max load = 2.1 kN Deflection at peak = 0.46

*** All compression specimens are 50.8×50.8×50.8 mm^3**
All OTEC specimens were made using ABS molds
PLA octet lattice unit cells were directly 3D-printed from PLA

Figure 7 - Flowchart of the experimental program.

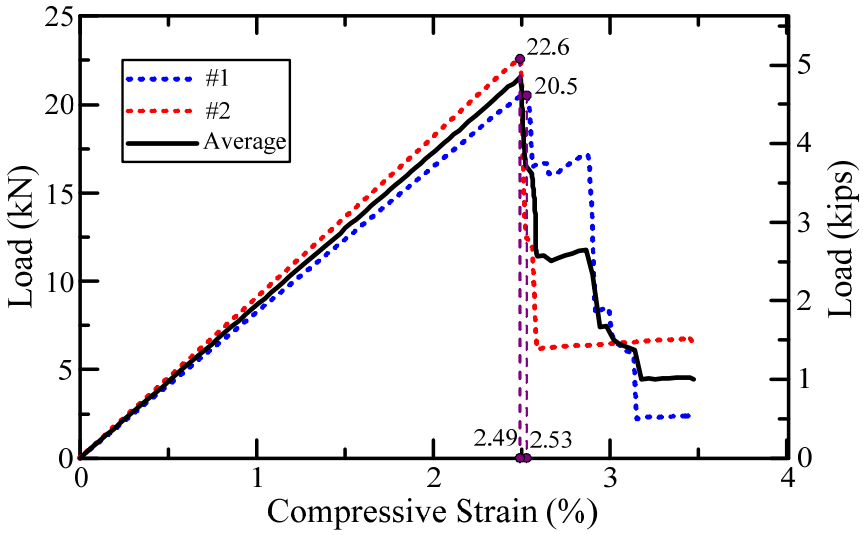
#1
#2
Average
22.6
20.5
2.49
2.53
Load (kN)
Load (kips)
Compressive Strain (%)

(a)

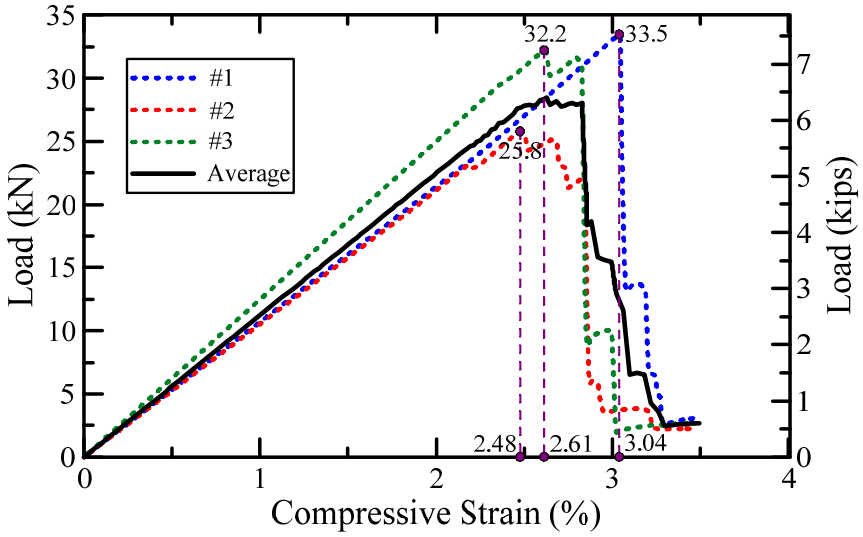
#1
#2
#3
Average
32.2
33.5
25.8
2.48
2.61
3.04
Load (kN)
Load (kips)
Compressive Strain (%)

(b)

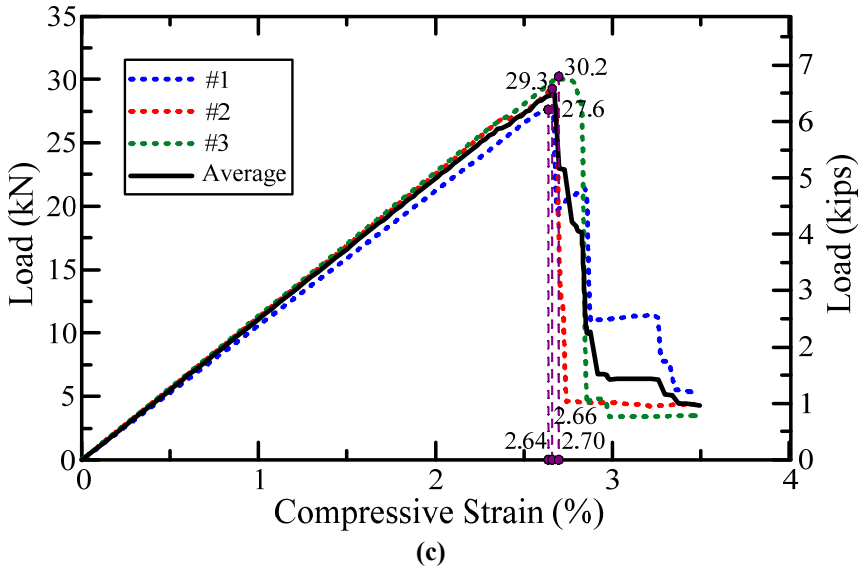

Figure 8 - Load–strain curves for 8 mm UHP-FRC OTEC unit cells (a) cured at room temperature and humidity, (b) placed in the fog room (with more than 95% relative humidity at room temperature), and (c) immersed in water until a day before testing, and (d) average load–strain curves for 8 mm UHP-FRC OTEC unit cells cured using three different methods (Experiment #3).

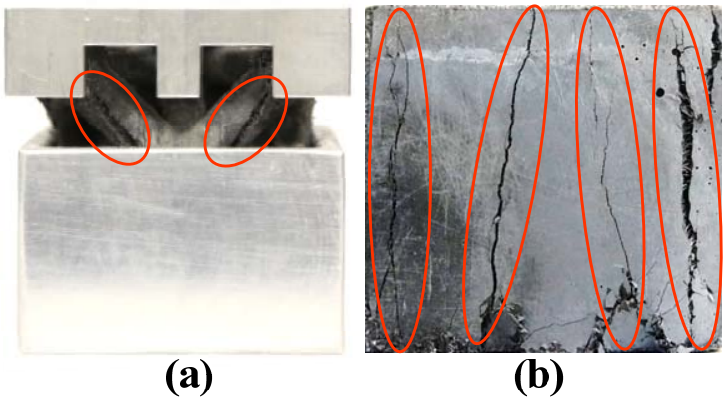

Figure 9 - (a) Formation of columnar cracks along the diagonal elements of the UHP-FRC OTEC unit cells and (b) vertical columnar cracks of 50.8-mm solid UHP-FRC cube specimens after testing under uniaxial compression.

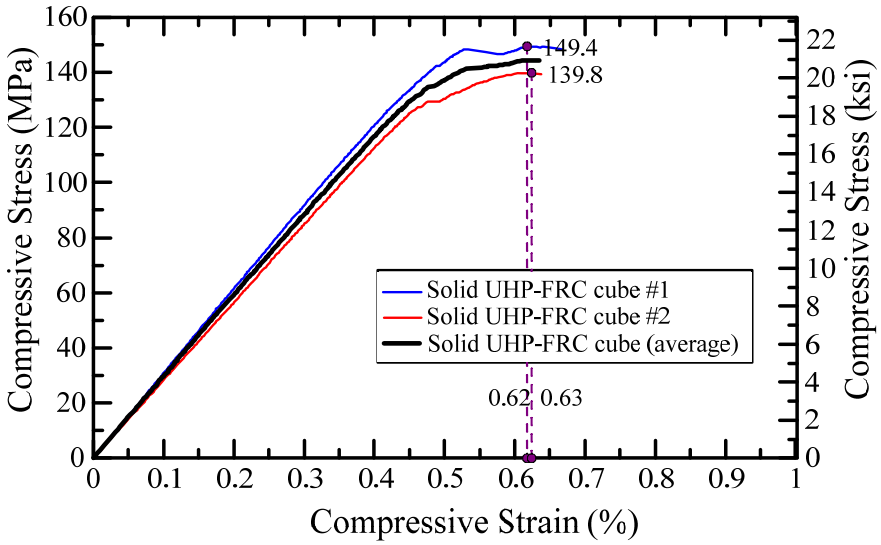

Figure 10 - Stress-strain curve of UHP-FRC with 0.5% volume fraction of PE fibers tested under uniaxial compression in Experiment #4.

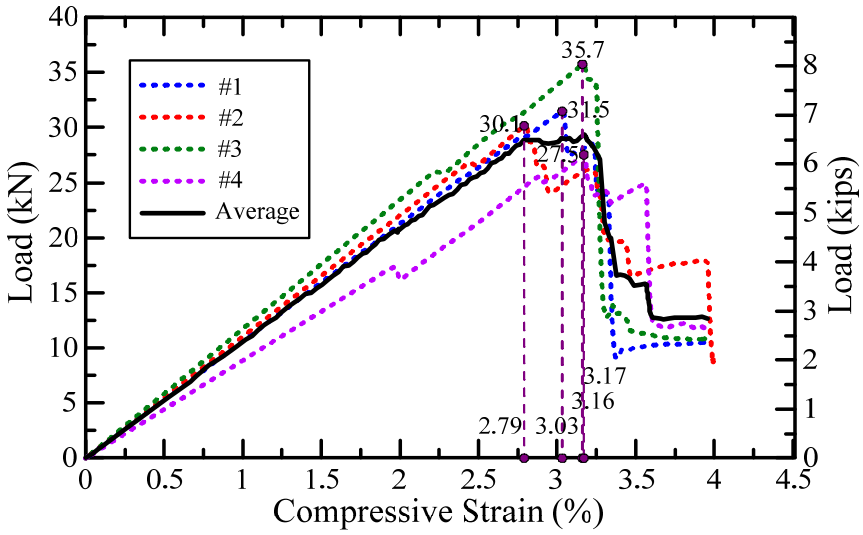
#1
#2
#3
#4
Average
35.7
31.5
30.1
27.5
3.17
3.16
2.79
3.03
Load (kN)
Load (kips)
Compressive Strain (%)

(a)

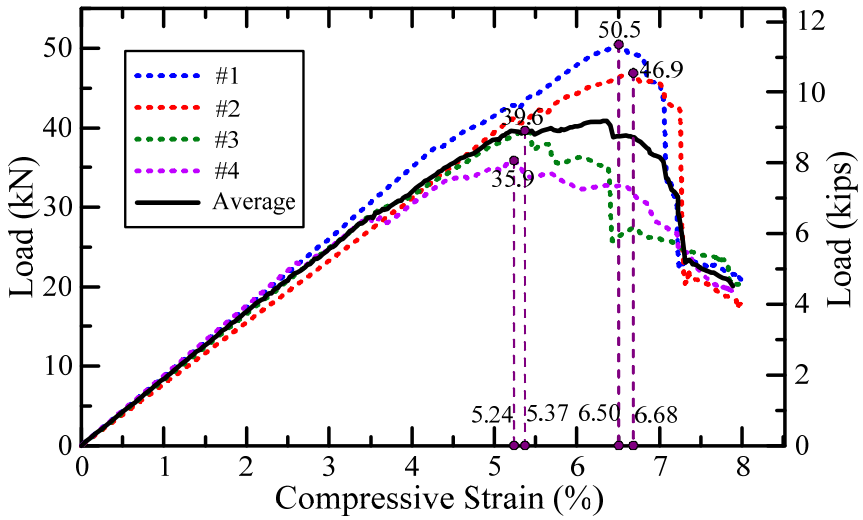
#1
#2
#3
#4
Average
50.5
46.9
39.6
35.9
5.24
5.37
6.50
6.68
Load (kN)
Load (kips)
Compressive Strain (%)

(b)

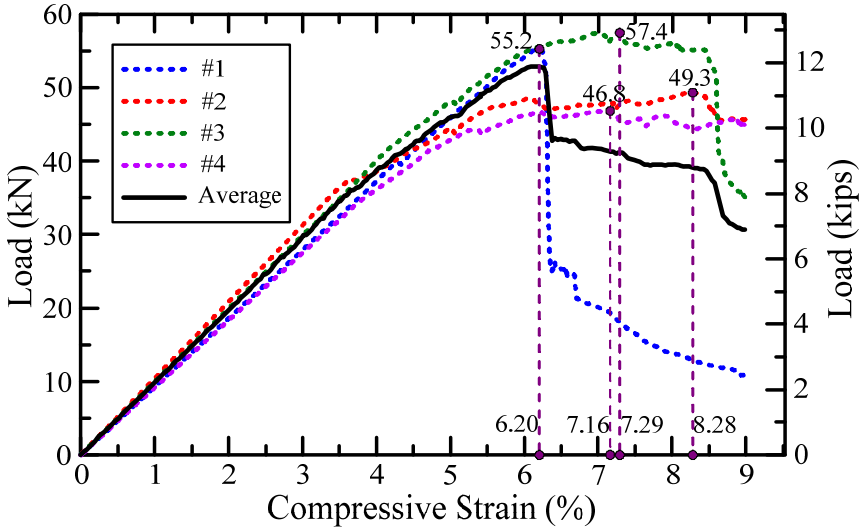

(c)

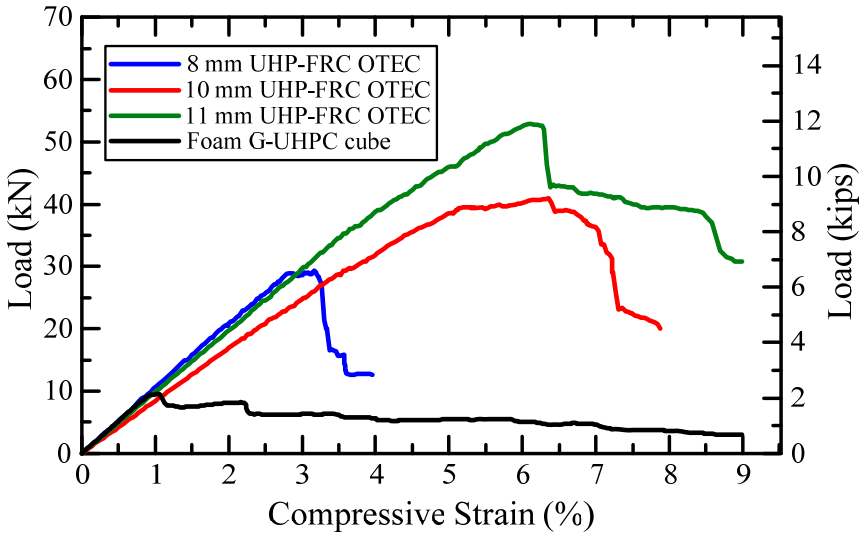

(d)

Figure 11 - Load-strain curves for (a) 8 mm, (b) 10 mm, (c) 11 mm UHP-FRC OTEC unit cells (d) all together with that of the foam G-UHPC cube (Experiment #1), tested under uniaxial compression (Experiment #4).

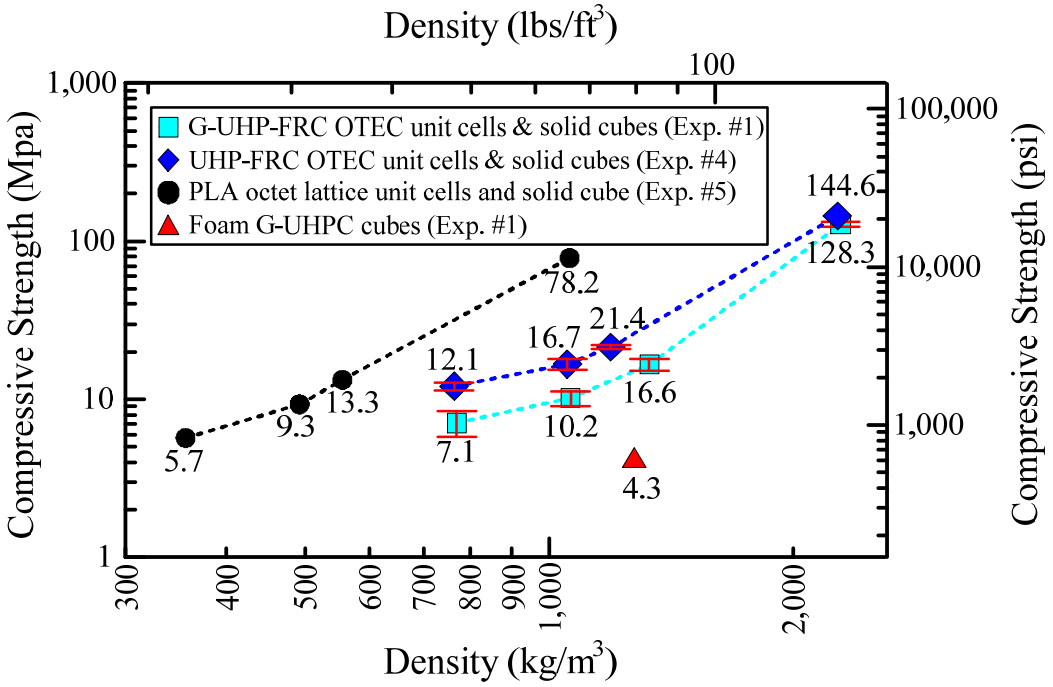

Figure 12 - Compressive strength versus density for octet lattice unit cells and foam G-UHPC and solid G-UHP-FRC and UHP-FRC cubes tested under Experiments #1, #4, and #5.

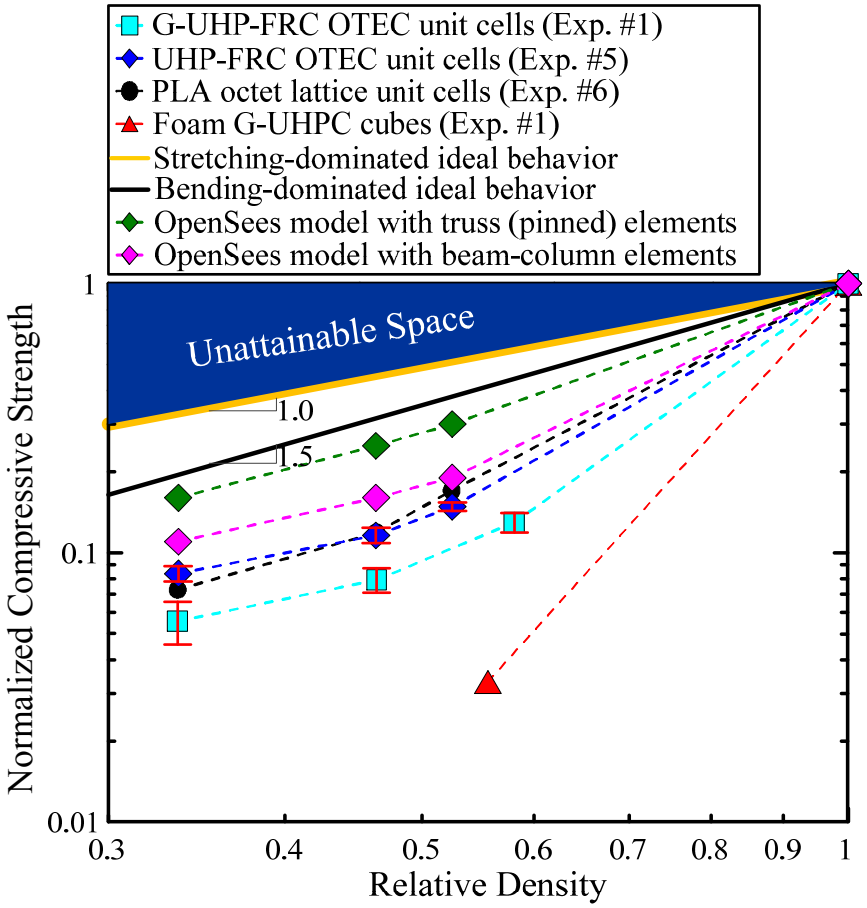

Figure 13 - Normalized compressive strength versus porosity for octet lattice cells and foam G-UHPC concrete tested under Experiments #1, #4, and #5 compared to the ideal behavior.

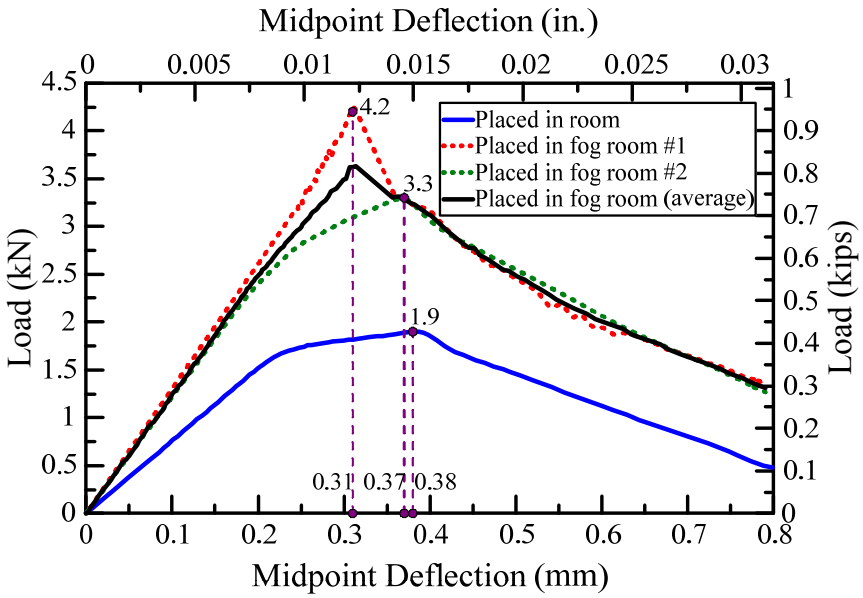

Figure 14 - Load–deflection curves of G-UHP-FRC 5×1×1-cell OTEC flexural material specimens under four-point bending at 28 days after casting.

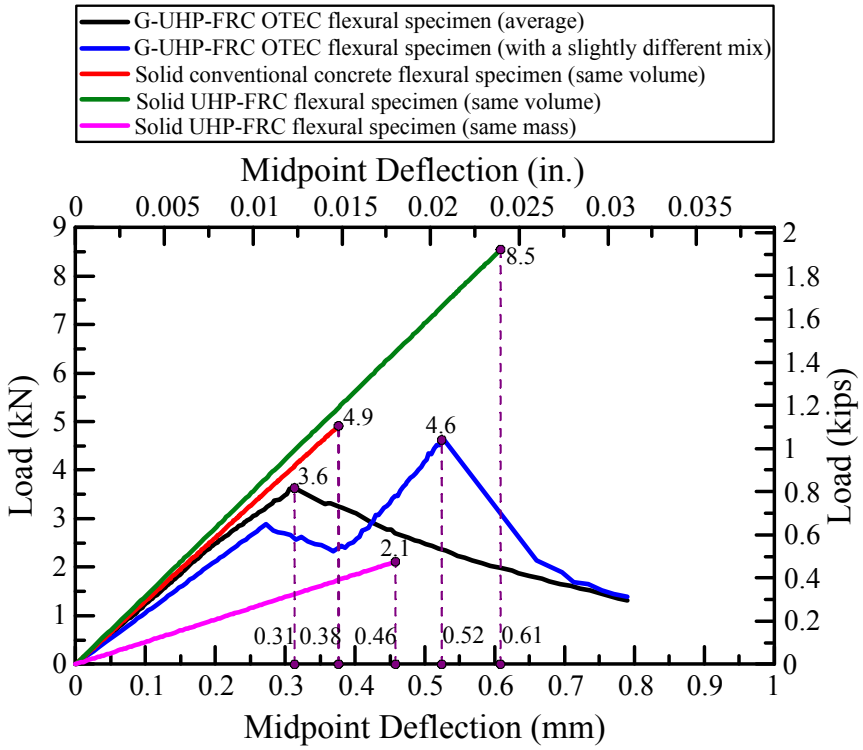

Figure 15 - Load–deflection curves of G-UHP-FRC 5×1×1-cell OTEC flexural material specimens compared with solid flexural control specimens (with either the same external volume [not the same material volume] or the same mass as those of the OTEC flexural specimens) under four-point bending at 28 days after casting.

Tables

Material	Description	Size*/Length (L)	G-UHP-FRC	UHP-FRC	Conventional Concrete†
Silica Sand 1 (S1)	460 Mesh	460 μm	0.7	0.6	0.0
Silica Sand 2 (S2)	120 Mesh	120 μm	0.3	0.3	0.0
Fine aggregate	90 Mesh	90 μm	0.0	0.0	2.05
Fiber‡	Polyethylene (PE)	38.4 μm / 3 mm	0.022′	0.005–0.016′	0.0
Cement (C)	Type II/V	15 μm	0.5	1.0	1.0
Fly Ash (FA)	Class F	10 μm	0.25	0.1	0.18
GGBFS″	-	15 μm	0.25	0.0	0.0
Glass Powder (GP)	White Micro Silica	1.8 μm	0.25	0.25	0.0
Silica Fume (SF)	Black Undensified	0.3 μm	0.0	0.25	0.0
	White Undensified	0.5 μm	0.25	0.0	0.0
HRWR‴	Polycarboxylate-based	-	0.02	0.02	0.0024
W/CM£	-	-	0.25	0.26	0.51
Flow diameter (mm)	-	-	254	224	254

* Median particle size
† Used in Section 2.6 and 3.2 as a control mix for comparison purposes
‡ High modulus, ultra-high molecular weight polyethylene fibers with a tensile strength and elastic modulus of 2.2–2.4 GPa and 73–79 GPa, respectively
′ 2.0, 1.5, 1.5, and 0.5–1.5% by volume, respectively
″ Ground granulated blast-furnace slag
‴ High-range water reducer
£ Water [W]/CM = [W/(C+FA+GGBFS+SF)]

Table 1 - Materials and mixture compositions used in the experimental program.

Specimen	Experiment #	Fiber V_f† (%)	Porosity (%)	Density (kg/m^3)	Peak Load (kN)				Compressive Strength (MPa)				Standard Error (MPa)	Average Strength (MPa)
					#1	#2	#3	#4	#1	#2	#3	#4		
8 mm OTEC	1╫	2.0	66.4	769	14.2	15.9	24.9	-	5.5	6.2	9.7	-	1.3	7.1
10 mm OTEC		2.0	53.6	1,063	31.3	21.7	25.7	-	12.1	8.4	10.0	-	1.1	10.2
12 mm OTEC		2.0	41.9	1,330	49.4	41.9	37.4	-	19.2	16.2	14.5	-	1.4	16.6
Solid cube‡		2.0	0.0	2,290	319.7	353.5	320.2	-	123.9	137.0	124.1	-	4.3	128.3
Foam cube‖		0.0	45.3	1,274	12.5	9.6	-	-	4.8	3.7	-	-	-	4.3
Solid cube‖		0.0	0.0	2,329	300.4	-	-	-	116.4	-	-	-	-	116.4
8 mm OTEC	2╪	0.5	66.4	772	15.7	13.9	-	-	6.1	5.4	-	-	-	5.7
Solid cube		0.5	0.0	2,298	289.4	302.3	273.8	-	112.1	117.2	106.1	-	3.2	111.8
8 mm OTEC		1.0	66.4	762	12.0	16.2	-	-	4.7	6.3	-	-	-	5.5
Solid cube		1.0	0.0	2,267	288.1	272.4	283.6	-	111.6	105.6	109.9	-	1.8	109.0
8 mm OTEC		1.5	66.4	750	12.0	12.9	-	-	4.7	5.0	-	-	-	4.8
Solid cube		1.5	0.0	2,233	274.7	276.4	268.7	-	106.4	107.1	104.1	-	0.9	105.9
8 mm OTEC′	3╪	0.5	66.4	763	20.5	22.6	-	-	8.0	8.8	-	-	-	8.4
8 mm OTEC″		**0.5**	**66.4**	**763**	**33.5**	**25.8**	**32.2**	**-**	**13.0**	**10.0**	**12.5**	**-**	**0.9**	**11.8**
8 mm OTEC‴		0.5	66.4	763	27.6	29.3	30.2	**-**	**10.7**	**11.3**	**11.7**	-	0.3	11.3
8 mm OTEC£	4╪	**0.5**	**66.4**	**763**	**31.5**	**30.1**	**35.7**	**27.5**	**12.2**	**11.7**	**13.8**	**10.7**	**0.7**	**12.1**
10 mm OTEC£		0.5	53.6	1,053	50.5	46.9	39.6	35.9	19.6	18.2	15.4	13.9	1.3	16.7
11 mm OTEC£		0.5	47.5	1,192	55.2	50.5	57.4	57.7	21.4	19.6	22.3	22.4	0.6	21.4
Solid cube£		0.5	0.0	2,270	385.5	360.8	-	-	149.4	139.8	-	-	-	144.6
8 mm PLA lattice cell	5	-	66.4	356	14.6	-	-	-	5.7	-	-	-	-	5.7
10 mm PLA lattice cell		-	53.6	492	24.0	-	-	-	9.3	-	-	-	-	9.3
11 mm PLA lattice cell		-	47.5	556	34.4	-	-	-	13.3	-	-	-	-	13.3
Solid PLA cube		-	0.0	1,060	355.5	-	-	-	-	-	-	-	-	-

***** Refer to Table 1
† Fiber volume fraction
‡ Tested after 225 days
′ Cured at room temperature and humidity
″ Cured in the fog room with more than 95% relative humidity at room temperature
‴ Immersed in water
£ Tested after 50 days
╫ G-UHP-FRC
╪ UHP-FRC
‖ G-UHPC

Table 2 - Compression test results of OTEC unit cells and foam and solid G-UHP-FRC and UHP-FRC cubes after 28 days (unless otherwise specified).

Experiment #	Specimen	Density (kg/m^3)	Compressive Strength (MPa)	Estimated Strength* (MPa)	Error (%)
1	8 mm G-UHP-FRC OTEC	769	7.1	3.0	-57.2
	10 mm G-UHP-FRC OTEC	1,063	10.2	9.1	-10.8
	12 mm G-UHP-FRC OTEC	1,330	16.6	19.4	17.0
	Solid G-UHP-FRC cube	2,290	128.3	122.2	-4.8
4	8 mm UHP-FRC OTEC	763	12.1	6.1	-49.9
	10 mm UHP-FRC OTEC	1,053	16.7	15.4	-7.7
	11 mm UHP-FRC OTEC	1,192	21.4	22.1	3.2
	Solid UHP-FRC cube	2,270	144.6	142.7	-1.3
5	8 mm PLA lattice cell	356	5.7	3.8	-32.8
	10 mm PLA lattice cell	492	9.3	9.4	0.7
	11 mm PLA lattice cell	556	13.3	13.1	-1.3
	Solid PLA cube	1,060	78.2	78.2	-0.1

* Based on a log–log regression using the last three data points

Table 3 - Estimated compressive strengths based on a log–log regression according to the data points corresponding to the 10 and 11 mm (or 12 mm) lattice cells and solid cubes.

Flexural specimen	Dimensions (mm^3)	Mass (g)	Peak load (kN)	Midpoint deflection at peak (mm)	Toughness (kN-mm)	Compressive strength (MPa)
G-UHP-FRC OTEC (average)	50.8×50.8×222.0	665.3	3.6	0.31	1.70	128.3*
G-UHP-FRC OTEC†	50.8×50.8×222.0	664.3	4.6	0.52	1.84	122.7*
Solid conventional concrete (same volume)‡″	50.8×50.8×222.0	1,207.1	4.9	0.38	0.92	36.5′
Solid UHP-FRC (same volume)″	50.8×50.8×222.0	1,262.8	8.5	0.61	2.60	143.5′
Solid UHP-FRC (same mass)‴	26.7×50.8×222.0	660.7	2.1	0.46	0.48	143.5′

* Refer to Table 2
† G-UHP-FRC with a slightly different mix design compared to that of Experiment #1, tested after 181 days
‡ Refer to Table 1
′ Average of three samples
″ This specimen had the same external volume (not the same material volume) as those of the OTEC flexural specimens for comparison purposes
‴ This specimens had the same mass as those of the OTEC flexural specimens for comparison purposes

Table 4 - Peak load, midpoint deflection at peak, and toughness values for the flexural specimens of Figure 15 under four-point bending at 28 days after casting.